Numerical analysis of downwash flow field from quad-rotor unmanned aerial vehicles

Haiyan Zhang[1,2], Yubin Lan[2,4*], Ningwen Shen[2,3], Jinyong Wu[2,3], Tao Wang[2,3], Jie Han[2,3], Sheng Wen[2,3]

(1. *College of Information and Electrical Engineering, Shenyang Agricultural University, Shenyang 110866, China*;
2. *National Center for International Collaboration Research on Precision Agricultural Aviation Pesticides Spraying Technology (NPAAC), South China Agricultural University, Guangzhou 510642, China*;
3. *College of Engineering, South China Agricultural University, Guangzhou 510642, China*;
4. *College of Electronic Engineering, South China Agricultural University, Guangzhou 510642, China*)

Abstract: Agricultural drones, also known as Unmanned Aerial Vehicles (UAV), have attracted increasing attention because of their advantages of small size, convenient handling, and the ability to function without a runway, and they are particularly suitable for small farmlands in Asia, especially in China. The downwash flow field caused by the rotors of agricultural drone is one of main characteristics and affects the droplet deposition and drift law. Studying the distribution characteristics and development law of the downwash flow field is the basis for improving the application performance of spray technology applied on agricultural drones. With the development of computational fluid dynamics, agricultural aerial spray modeling has become an area of academic interest. In this study, the numerical simulation method was used to calculate the downwash flow field model of the quad-rotor UAV, to analyze its distribution characteristics and development law over time at different flight speeds. The accuracy of the numerical simulation was verified by field test. The simulation results show that the average velocities of airflow under 1.6 m from rotors at 2, 4 and 6 m/s are 2.33 m/s, 1.90 m/s and 1.03 m/s, respectively, which are high enough to disturb most of plant canopy and enhance the penetration rate of droplets. The flight velocity of drone has a significant effect on the downwash flow field. With the increase of the flight velocity, the wake of drones is gradually raised, and the concentration of wingtip vortices increases. When the flight velocity is increased to 6 m/s, the wingtip vortex velocity reaches 3.3 m/s, which has a strong entrainment effect on the droplets and greatly increases the risk of droplet drift.

Keywords: quad-rotor UAV for plant protection, agricultural drones, downwash flow field, flight velocity
DOI: 10.33440/j.ijpaa.20200304.138

Citation: Zhang H Y, Lan Y B, Shen N W, Wu J Y, Wang T, Han J, Wen S. Numerical analysis of downwash flow field from quad-rotor unmanned aerial vehicles. Int J Precis Agric Aviat, 2020; 3(4): 1–7.

1 Introduction

Crop spraying is a critical, expensive, and time-consuming labor activity in agricultural production. Thus, the use of aircraft to perform this task is becoming increasingly prevalent, owing to their speed and effectiveness in spraying operations. For this purpose, agriculture drones or Unmanned aerial vehicles (UAVs) have attracted increasing attention because of their advantages of small size, convenient handling, and the ability to function without a runway, and they are particularly suitable for small farmlands in Asia[1]. With a few years development, agriculture drones have been used widely in modern precision agriculture. The use of UAVs has progressed particularly rapidly in East Asia for their excellent application efficiency and ability to protect densely planted crops, especially in China[2,3]. The survey result conducted by the National Agricultural Technology Extension Center of Ministry of Agriculture and Rural Affairs showed that there were more than 50,000 plant protection drones and 4,670,000 mu cultivated field were sprayed in China in 2019[4]. Nowadays, the spray technology applied on UAVs has developed into one of main plant protection technology in China.

The downwash flow field caused by the rotors of agriculture drone is one of its main characteristics and affects the droplet deposition and drift law. Studying the distribution characteristics and development law of the downwash flow field is the basis for improving the application effect of spray technology applied on agriculture drones[5,6]. Li et al.[7-10] developed a wireless wind speed sensor network measurement system for agriculture drones. Based on this wind speed sensor network measurement system, Wang et al.[11] measured the wind speed, wind direction and the downwash flow field width of Z3 single-rotor UAV during pollination operations, and analyzed the effect of flight height, the flight direction and natural wind direction on the downwash flow field width. This research provides a reference for the operation parameters selection of UAV in pollination operation. Li et al.[12-14] obtained the coupled wind field parameters between the downwash flow field induced by rotors and rice canopy when single-rotor, 8-rotor and 18-rotor UAV for plant protection were

Received data: 2020.11.01 **Accepted data**: 2020-12-09
Biographies: Haiyan Zhang, PhD Student, research interests: Precision Agriculture Spray Technology, Email: 1322366847@qq.com; **Ningwen Shen**, Postgraduate, research interest: Precision Agriculture Spray Technology, Email: 2846833826@qq.com; **Jinyong Wu**, Postgraduate, research interests: Precision Agriculture Spray Technology, Email: 1404542660@qq.com; **Tao Wang**, Postgraduate, research interests: Precision Agriculture Spray Technology, Email: 1753018668@qq.com; **Jie Han**, Postgraduate, research interest: Precision Agriculture Spray Technology, Email: 2048570351@qq.com. **Sheng Wen**, PhD, Associate Processor, research interests: Precision aviation spray technology, Email: vincen@scau.edu.cn.

* **Corresponding author: Yubin Lan**, PhD, Professor, interests: Precision Agriculture Spray Technology. Mailing Address: South China Agricultural University, Wushan Road, Tianhe District, Guangzhou City, Guangdong, 510642, China. Email: ylan@scau.edu.cn.

used for rice pollination operations, including the wind speed in three directions of rice canopy X, Y and Z, wind field width and the highest wind speed characteristics. According to the parameters of wind field, Li et al. analyzed the effect of operational height, speed and UAV load on the distribution characteristic.

The above-mentioned researches were conducted based on field test methods. Field tests are carried out in a real operating environment. The test result can more truly reflect the effect of the wind field caused by UAV on the deposition and drift of droplets. However, due to the complex nature of the field environment, there may be many random natural factors in the test process. Limited by current test equipment and methods, it is temporarily impossible to eliminate the influence of field random factors on the field test results. In addition, due to the limitations of test costs and test method, although field trials can obtain more realistic results of the impact of the wind fields on droplet deposition and drift, field trials have not yet been able to obtain the overall morphology of the wind field, the development law of the rotor wind field over time, and the details of the local vortex.

With the development of computational fluid dynamics, agricultural aerial spray modeling has become an area of academic interest. Liu [15] took LTH-100 single rotor UAV as the research object, simulated the downwash flow field characteristics of UAV in hover and forward flight under different lateral wind conditions, and verified the accuracy of the numerical model by wind speed distribution test. The results showed that the airflow began to wind up and downwash flow field became complicated when the airflow developed 2 meters under rotor of UAV. And it is recommended that UAV's operating altitude be less than 2 m. Tang et al[16] used large-eddy simulation and lattice Boltzmann method to simulate the downwash flow field and the droplet movement law and verified the accuracy of the numerical model by the wind speed obtained by[17,18]. The results showed that the downwash flow field was asymmetric, and the increase of the flight height would aggravate the asymmetry of the downwash flow field, which caused the asymmetric of droplet deposition. With the flight height increasing, the coefficient of variation of the droplet deposition decreases and the quality of the droplet deposition decreases. Wen et al.[19] simulated the flow field under a single-rotor UAV based on an adaptive thinned physical model of the lattice Boltzmann method, and captured accurately the trajectories of droplet with different droplet diameters based on the Lagrange discrete particle tracking method. The results showed that as the UAV flight speed was greater than 3 m/s, a spiral tail vortex appeared at the rear of the fuselage. And 38% of droplets were drifted by the spiral tail vortex at the flight 5 m/s and the flight height of 3 m, in which 80% of the drifted droplets was smaller than 100 μm. Yang et al.[20] established the three-dimensional numerical model for six-rotor UAV under 3 kg load condition and analyzed the influence of the downwash flow field on the motion distribution of droplet group. The results showed that the "shrinkage-expansion-shrinkage" appeared in the longitudinal main section, due to the rotation of airfoil and extrusion of the external atmospheric pressure. The "airflow inlet" and "airflow outlet" region appeared between the wings area at the cross section. When the droplet diameter was less than 200 μm, the droplet movement range could not cover all the "airflow inlet" area, and the droplets were mostly distributed in the center down wash area. When the diameter was greater than 250 m, the droplet motion region gradually covered all the "airflow inlet" and "airflow outlet". Zhang et al.[21] simulated the airflow field induced rotor of six-rotor UAV based on computational fluid dynamics method, combined with RNG k-ε turbulence model, porous model and sliding mesh technology, and analyzed the effect of hovering heights of UAV, fruit growth stages and natural wind speeds on the airflow field characteristic. The results showed that natural wind changed the symmetry of the airflow field of UAV; and with the increase of the hovering height and natural speed, the trail distance of airflow field enhanced.

The above-mentioned papers calculated the downwash flow field of single-rotor and six-rotor UAVs, analyzed the droplet movement law based on numerical simulation methods, preliminarily obtained the distribution characteristic of the downwash flow field and its development law over time. Quad-rotor UAVs are also widely used in china, so it's necessary and worthy to study the downwash flow field characteristic of quad-rotor UAV. In this paper, the numerical simulation method is used to calculate the downwash flow field model of the quad-rotor UAV, analyzed its distribution characteristic and development law over time at different flight speeds. The accuracy of the numerical simulation was verified by field test.

2 Materials and methods

2.1 Quad-rotor UAV 3D model

In this paper, the P20 type quad-rotor UAV (Guangzhou XAG) is selected as a model for the numerical analysis, whose detailed parameters are shown in Table 1.

Table 1 The detailed parameters of P20 quad-rotor UAV

Parameters	Values	Remarks
Maximum flight speed/m·s^{-1}	12	Autonomous setted
Maximum flight altitude/m	4000	Autonomous setted
Size of P20/mm	1852/1828/403	Length/width/Height
Takeoff weight/kg	32	Max weight
Push-to-weight ratio	2.14	Max weight

It's extremely important to build the model accurately, which decide the accuracy of the numerical analysis. The rotor, induced downwash flow field, is the core part of UAV. Because the rotor surface is very complex, it's difficult to build its 3D model directly. The 3D optical scanner VisenTOP (Tianjin Vision Sensitive Technology Co., Ltd, China) was used to scan the rotors of P20. Then, the 3D model of rotor was rebuilt by using the Geomagic Studio software (Geomagic Inc.), as shown in Figure 1. The fuselage, pesticide cabinet, and nozzles were modeled in Autodesk Inventor Professional 2016 (AutoDesk, America). The eventual 3D model of P20 is shown in Figure 2a.

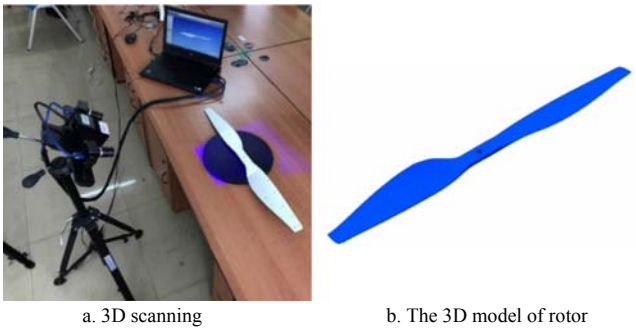

a. 3D scanning b. The 3D model of rotor

Figure 1 The 3D scanning process of rotor

The definition of the coordinate system is shown in Figure 2a: define the positive direction of the X axis as the forward direction of the P20 UAV, the positive direction of the Y axis as the rising direction of the P20 UAV, and the positive direction of the Z axis as

the P20 UAV body from left to right direction. The rotor rotation direction is defined as shown in Figure 2b. Rotor one and rotor three are defined as counterclockwise rotation. Rotor two and rotor four are defined as clockwise rotation.

a. P20 3D model

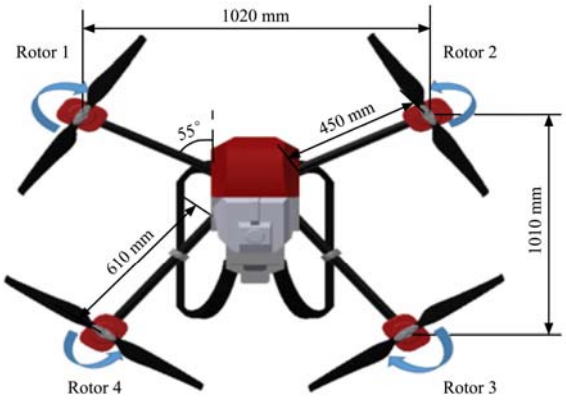

b. Bhe rotation direction of rotors

Figure 2 P20 3D model and the rotation direction of rotors

2.2 Numerical method

2.2.1 Lattice Boltzman method

Lattice Boltzmann Method (LBM) is a computational fluid dynamics method at a mesoscopic simulation scale. Compared with other CFD calculation methods, LBM does better in calculating the flow field with complex boundary and non-stationary movement object. And it could accurately deal with the problem on the micro and macro scales, So it's more suitable to calculate the downwash flow field of UAV.

The calculation domain of the LBM is a uniform cubic element, and the characteristic lattice structure of the element is D3Q27, as shown in Figure 3. There are 27 discrete velocity vectors, including one velocity vectors, positioned at the center of the lattice, is zero; six discrete velocity vectors from the domain center to the lattice center; 12 discrete velocity vectors from the body center to the midpoint of the edge of the lattice, and 8 discrete velocity vectors from the body center to the top angle of the lattice.

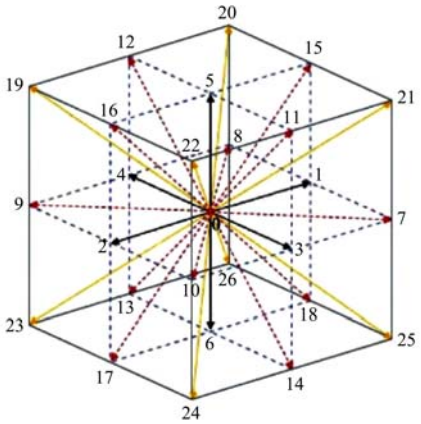

Figure 3 Lattice of D3Q27 model

2.2.2 Turbulence modeling

The Large eddy simulation model (LES) used in XFlow is the wall-adapting local-eddy viscosity (WALE) model. Because the spatial resolution is not very high in the boundary layer, the WALE model is used to conserve computational resources. The WALE model is formulated as follows:

$$\upsilon_t = \Delta_f^2 \frac{(G_{\alpha\beta}^d G_{\alpha\beta}^d)^{\frac{3}{2}}}{(S_{\alpha\beta}S_{\alpha\beta})^{\frac{5}{2}} + (G_{\alpha\beta}^d G_{\alpha\beta}^d)^{\frac{5}{4}}} \quad (1)$$

and

$$\Delta_f = c_w \Delta \quad (2)$$

$$S_{\alpha\beta} = \frac{g_{\alpha\beta} - g_{\beta\alpha}}{2} \quad (3)$$

$$G_{\alpha\beta}^d = \frac{1}{2}(g_{\alpha\beta}^2 + g_{\beta\alpha}^2) - \frac{1}{3}\delta_{\alpha\beta}g_{\gamma\gamma}^2 \quad (4)$$

where, v_t is the modeled eddy viscosity; Δ_f is the filter scale; c_w is a constant with value 0.325; Δ is the grid volume; $S_{\alpha\beta}$ and $G_{\alpha\beta}$ are strain-rate tensor of the resolved scales; $\delta_{\alpha\beta}$ is Kronecker symbol; $g_{\alpha\beta}$, $g_{\beta\alpha}$ and $g_{\gamma\gamma}$ are the strain-rate tensor. α, β and γ represent space direction, and in the three-dimensional, α, β and $\gamma$are the one, two and three, respectively.

2.2.3 Computational domain and boundary conditions

The virtual wind tunnel is select as the computational domain, whose size was 40×5×8 m in X, Y, Z direction, as indicated in Figure 4. The P20 model is positioned in the virtual wind tunnel at height of 2 m from the ground.

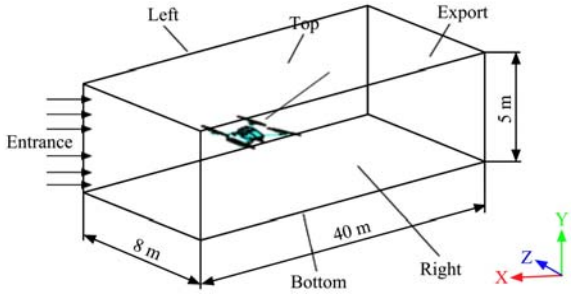

Figure 4 The computational domain

In order to calculate the downwash flow field of P20 accurately, it's necessary to improve the spatial and temporal resolution of the computational domain. Since the refinement of the simulation focuses on the rotor surface, the surface of the fuselage, and the wake of the downwash flow field, in order to save computing resources, the global spatial refinement resolution size of the virtual wind tunnel is set to 0.05 m. The surface refinement algorithm of the fuselage and rotor is set as an adaptive method. The refinement resolution size of the fuselage is set to 0.05 m, and the refinement resolution size of the rotor is set to 0.025 m. In order to capture the characteristics of the wake of the downwash flow field, the refinement resolution size of the wake is set to 0.0125 m, and the wake refinement threshold is set to 1×10^{-5} m. The effect diagram of automatic discretization after parameter setting is shown in Figure 5.

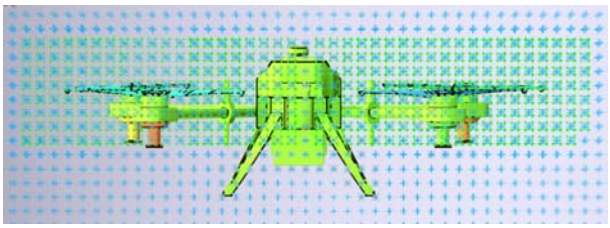

Figure 5 Discretization of computational domain

2.3 Field test

To verify the accuracy of the numerical results, a field test was conducted. Because the instantaneous velocity field in the forward-flight application could not be determined owing to experimental limitations, the hovering case were selected in the verified test.

Because the fuselage of UAV has little effect on the downwash flow field of rotor, a mimic UAV system, shown in Figure 6a, was used to replace the P20 in the verified test. However, the rotor, caused downwash flow field applied on P20, the core component, are placed on the mimic UAV system and used to induced the downwash flow field.

During the verified test, the mimic UAV system was set at 2 m from the ground, and the rotation speed of rotors is 2450 r/min. Which is equal to the numerical simulation. When the downwash flow field developed steadily, 8 test samples are measured by anemoscope at 1m from the ground. As shown in Figure 6b, the 8 samples are the four points directly below the rotor and the position below the center point between adjacent rotors. The airflow velocity is obtained by the numerical simulation at same position with field test and shown in Table 2. Figs. 6c, 6d and 6e show the velocity distribution cloud diagrams of the xoy, yoz and xoz sections when the drone is hovering. In Table 2, the wind speed error is within 8%, indicating that the numerical calculation basically meets the accuracy requirements of engineering calculations.

a. Downwash flow field wind speed test site

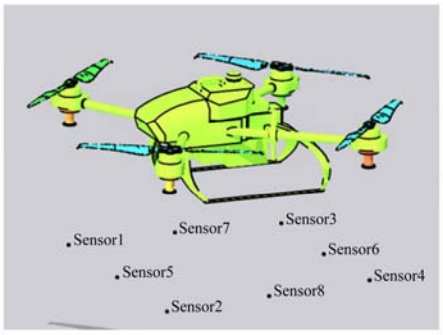

b. Location distribution of wind speed collection points in downwash wind farm

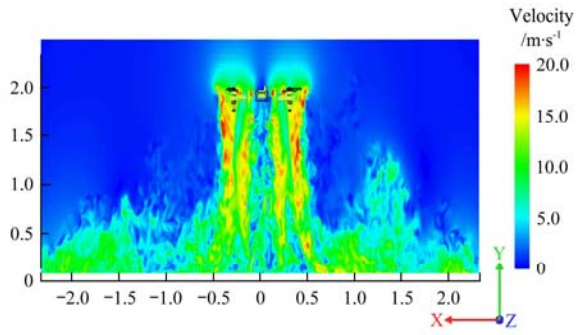

c. xoy Sectional wind speed distribution

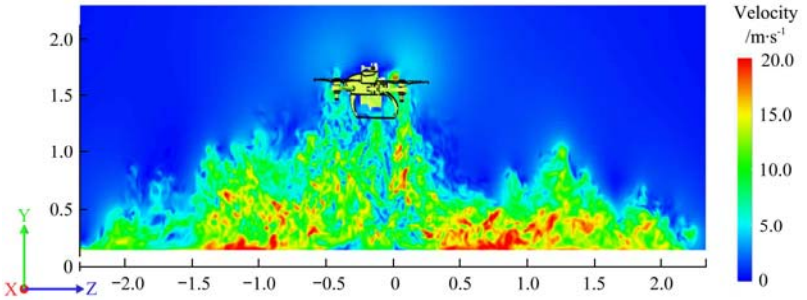

d. yoz Sectional wind speed distribution

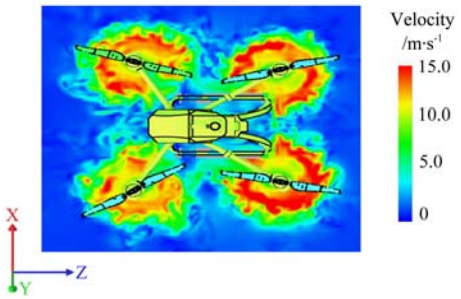

e. xoz Sectional wind speed distribution

Figure 6 Airflow test and numerical calculation results of flow field at 1.08 s under hovering conditions

Table 2 Experimental measurements and calculation values of velocity for marked points

Height /m	Sensor1			Sensor2			Sensor3			Sensor4		
	Calcuation /m·s^{-1}	Test /m·s^{-1}	Error /%	Calcuation /m·s^{-1}	Test /m·s^{-1}	Error /%	Calcuation /m·s^{-1}	Test /m·s^{-1}	Error /%	Calcuation /m·s^{-1}	Test /m·s^{-1}	Error /%
1	14.044	13.456	4.37	11.443	12.100	5.74	13.003	12.562	3.51	11.101	10.687	3.87
	Sensor5			Sensor6			Sensor7			Sensor8		
1	3.085	2.921	5.61	5.318	5.101	4.25	7.352	7.001	5.01	5.762	5.433	6.06

3 Results and analysis

3.1 Flow structure at different velocities

The instantaneous wake structure of P20 at different time is shown in Figure 7. When $t = 0.005$ s (Figure 7a), incomplete vortex ring is generated. When $t = 0.025$ s, complete vortex ring is developed gradually, as shown in Figure 7b. The vortex is almost symmetric along the X-axis direction. When $t = 0.045$ s (Figure 7c), vortex ring begins to be developed backward along the X-axis direction, the development of the downstream vortex starts to be affected by the upstream vortex. When $t = 0.065$ s (Figure 7d), the initial vortex ring is blown away from the rotor and the vortex shaped like a horseshoe is preliminarily formed. The vortex described above can carry droplet and affect the effective deposition of droplet on the target[19]. Figure 8 shows the downwash flow field of P20 at different flight velocity and pitch angle. When the UAV flies at 1 m/s, the airflow induced by rotors spreads to the ground spirally and almost perpendicularly. When the downwash airflow reaches the ground, the airflow starts to diffuse around the fuselage sides and rolls upward, duing to the ground effect. With the increasing of flight velocity, the whole downwash flow field is gradually lifted. The diffusion distance of wake to the fuselage is also gradually increased, the distance to the front of the fuselage is shortened. When the flight velocity is 6 m/s, there is no forwardly diffused airflow in the front of the UAV. Under the effect of relative airflow, the whole downwash flow field spreads backward as a whole.

Due to the difference in the pressure and flow velocity of the

airflow above and below the wing surface, a wingtip vortex is generated at the wingtip of the UAV, as shown in Figure 8. The wingtip vortex hangs above the rotor wake and develops backward in a spiral form, forming a vortex, the vortex is one of the main reasons for the upward movement of the droplets and the drift[22]. When the flight speed is 1-2 m/s, the vortex in the wake of P20 is not obvious. When the flight speed increases to 3 m/s, the vortex concentration began to increase significantly. As the flight velocity increases, the downwash flow field is gradually raised, and it couples with the wingtip vortices earlier, forming more vortices and increasing the downwash flow field Complexity.

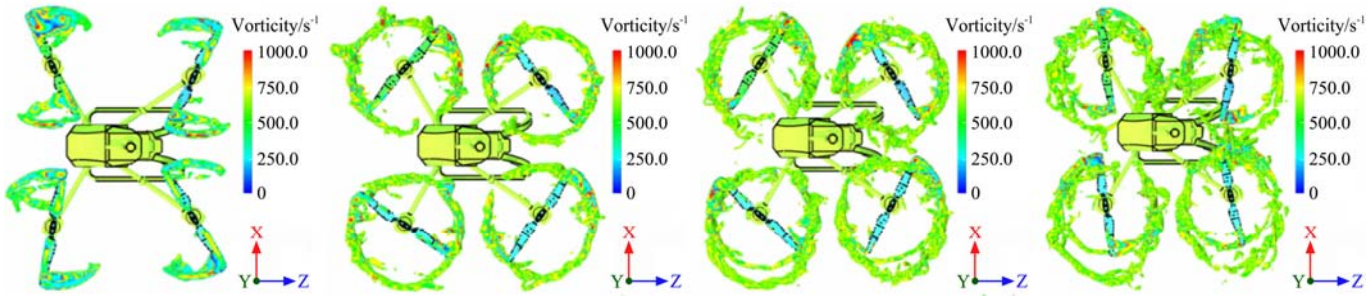

a. 0.005 s b. 0.025 s c. 0.045 s d. 0.065 s

Figure 7 The development of downwash flow field

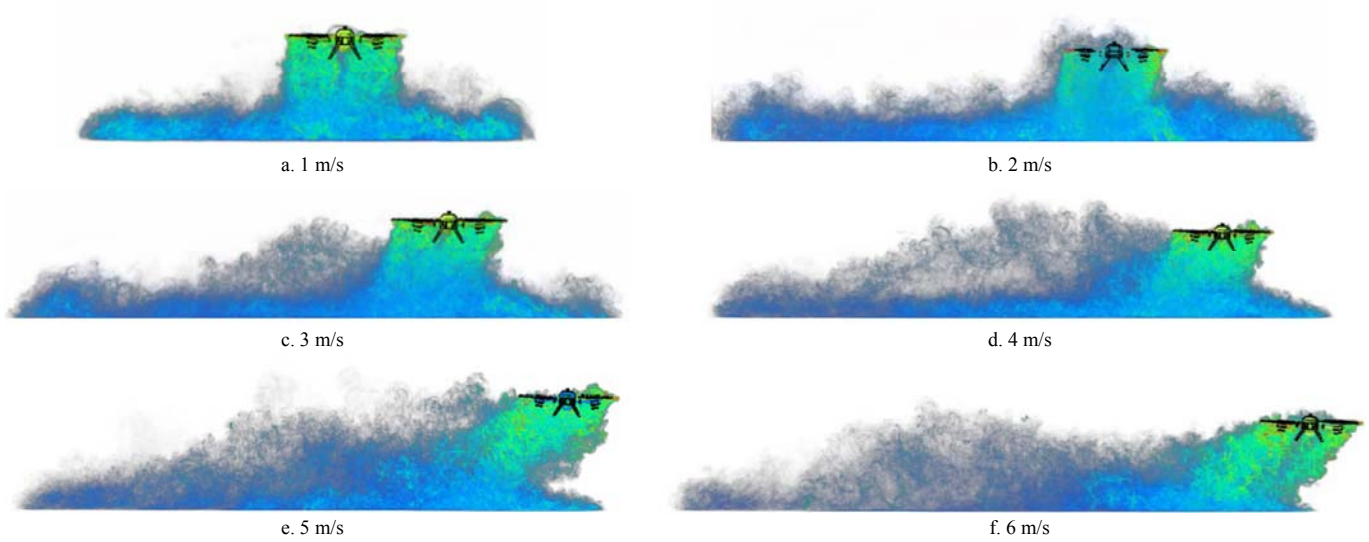

a. 1 m/s b. 2 m/s

c. 3 m/s d. 4 m/s

e. 5 m/s f. 6 m/s

Figure 8 The downwash flow field of P20 at different flight velocity

Figure 9 shows the velocity vectors at several planes downstream of P20 (0, 3, 6 and 7.5 m) when the flight velocity is at 2, 4 and 6 m/s, respectively. 0 m represents the velocity vector of the downwash flow field at the central section of the fuselage; 3 m, 6 m, and 9.5 m represent the velocity vector diagram on the cross section 3 m, 6 m and 9.5 m from the center of the fuselage, respectively. When the flight velocity is 2 m/s, when the wake of P20 spreads to 6 m behind the fuselage, the vortex that entrains the droplets moving upward has disappeared, as shown in Figure 9a. When the flight velocity increases to 4 m/s, and the wake spreads to 6 m behind the fuselage, the height of wake diffusion increases slightly, but the vortex has almost disappeared (Figure 9b). However, at 3 m behind the fuselage, the vortex concentration increases. Although the speed of the vortex varies from 0 to 5 m/s, it is enough to have impact on the droplet deposition. When the flight velocity of P20 is increased to 6 m/s, compared to the previous two cases, the wake concentration of the drone is greatly increased and the vortex has expanded to 9.5 m behind the fuselage, and there is still a certain amount of horseshoe-shaped wingtip vortices around the fuselage. It can be predicted that when the flight velocity of the UAV increases to 6 m/s, the amount of droplets moving upwards carried by the wingtip vortex increases sharply, and more droplets stay in the air for a longer time, prompting the droplets to drift.

The Y-direction airflow in the downwash flow field has the effect of assisting the droplet deposition. To analyze the influence of the UAV flight velocity on the Y-direction airflow velocity distribution, velocity sensor is set at 0.4 m, 0.8 m, 1.2 m and 1.6 m below the drone rotor when the flight velocity is 2, 4 and 6 m/s, respectively. The velocity sensor positions are shown in Figure 10. The Y-direction velocity distribution curves at various positions under the UAV rotor are shown in Figure 11.

Y-direction airflow velocity distribution is asymmetrical W-shape, which indicates that the airflow velocity generated by the adjacent rotors is not exactly the same. The airflow velocity generated by the rotor on the left side of the fuselage is greater. This will make the moving velocity of droplets on both sides of the drone different, which will easily lead to uneven deposition of droplets on both sides of the drone. Figure 11 shows that when the UAV flight velocity is 2 m/s, there are almost no wingtip vortices in the flow field. When the UAV flight velocity increases to 4 m/s, the wingtip vortices in the flow field increase, but not enough obviously. When the flight velocity increases to 6 m/s, the wingtip vortices on both sides of the rotor obviously increase, and the maximum upward movement speed of the wingtip vortices reaches 3.3 m/s, which has a very strong entrainment effect on the droplets, which greatly increase the risk of fog droplets drift.

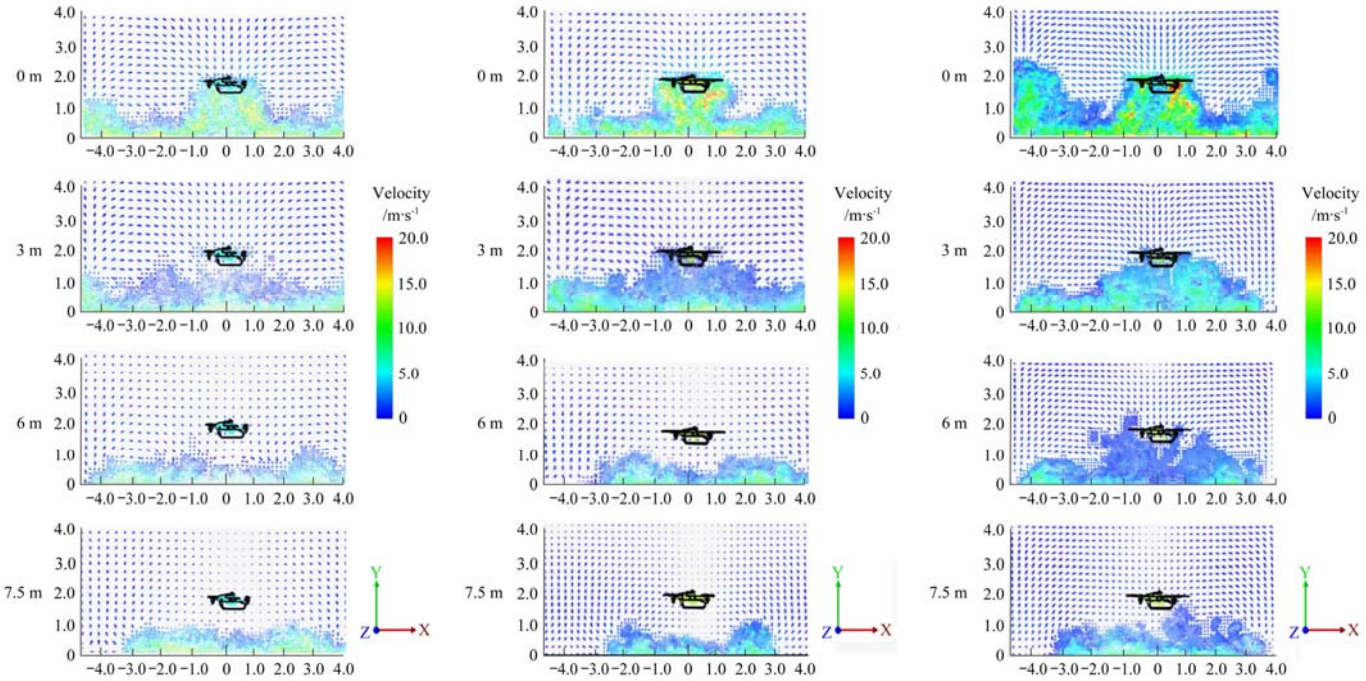

a. 2 m/s b. 4 m/s c. 6 m/s

Figure 9 Velocity vectors at several planes downstream of P20 (0, 3, 6 and 7.5m)

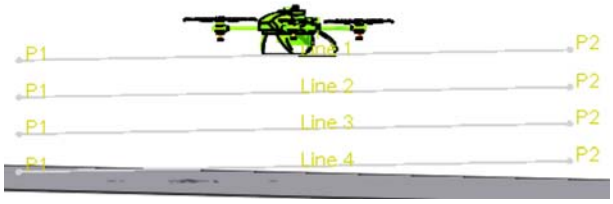

Figure 10 The position of velocity sensor plot line

When the distance from the rotors increases from 0.4 m to 0.8 m, the maximum Y-direction velocity of flow field at three flight velocity (2, 4 and 6 mm/s) increases by A, B and C, respectively. When the distance continues to increase from 0.8 m to 1.2 m, the Y-direction velocity decreases, and the upward Y-direction airflow, consisting of wingtip vortex and the airflow induced by the ground effect, appears gradually from both sides of the rotor. When the distance reaches 1.6 m, the upward Y-direction airflow increases sharply, and the maximum Y-direction velocity reaches 5.4 m/s, which is enough to disturb the plant disturb, affect the interaction process between the droplets and plant canopy, and further affect the droplet deposition.

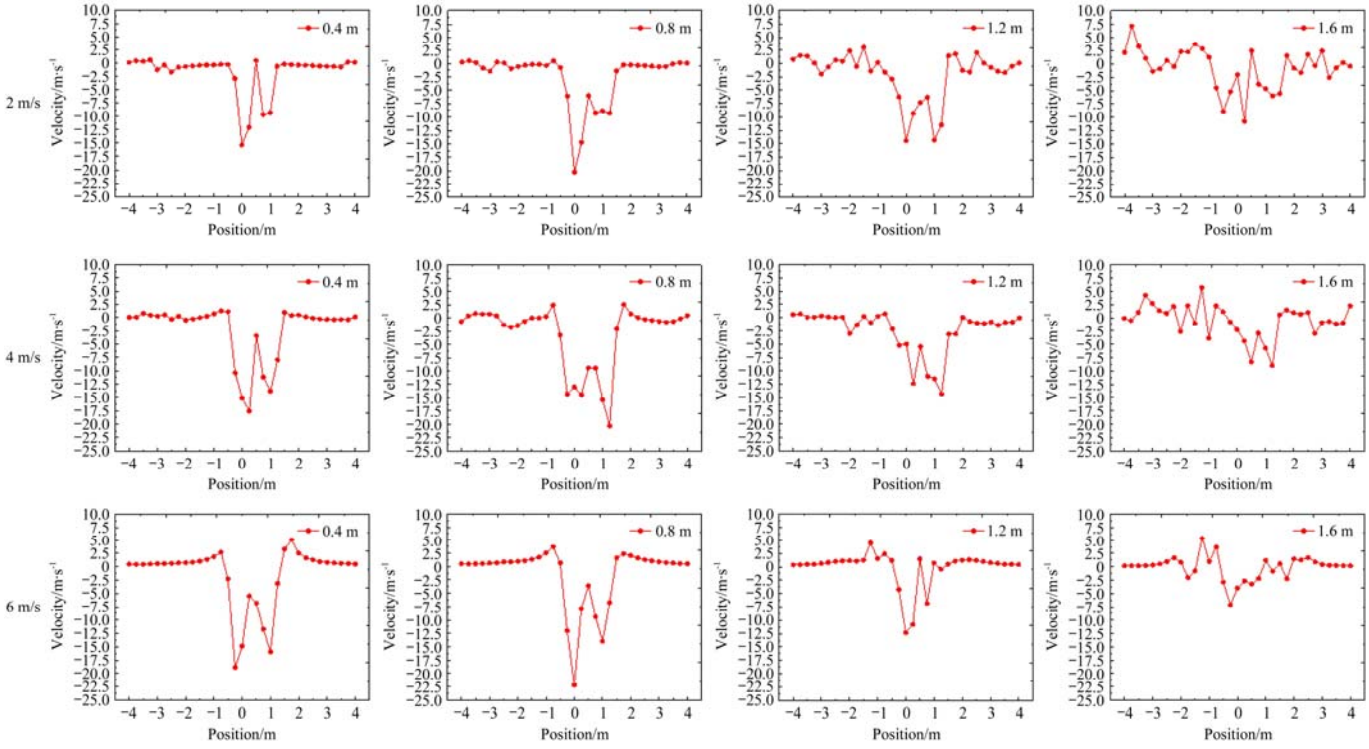

Figure 11 The Y-direction airflow velocity distribution curve

4 Conclusions

Based on the lattice Boltzmann method, this study simulates the downwash flow field of P20 quad-rotor UAV at different flight speeds, and verifies the accuracy of this method by the field test. The following conclusions are drawn:

(1) The average velocities of airflow under 1.6 m from rotors at 2, 4 and 6 m/s are 2.33 m/s, 1.90 m/s and 1.03 m/s, respectively, which is high enough to disturb most of plant canopy and enhance the penetration rate of droplet.

(2) The flight velocity of drone has a significant effect on the downwash flow field. With the increase of the flight velocity, the wake of drones is gradually raised, and the concentration of wingtip vortices increases. When the flight velocity increases to 6 m/s, the wingtip vortex velocity reaches 3.3 m/s, which has a strong entrainment effect on the droplets and greatly increases the risk of droplet drift.

[References]

[1] Lan Y, Chen S , Fritz B K. Current status and future trends of precision agricultural aviation technologies. Int J Agric Biol Eng, 2017; 10(3): 1–17. doi: 10.3965/j.ijabe.20171003.3088

[2] Zhang D, Lan Y, Chen L, et al. Current status and future trends of agricultural aerial spraying technology in china. Transactions of the Chinese Society for Agricultural Machinery, 2014; 45(10): 53–59.

[3] Guo Y, Wang N, Jin B. Development status of unmanned aircraft for agricultural plant protection. Agricultural Engineering, 2017; 7(2): 24–25.

[4] Cheng Z. Annual Development Report of Plant Protection UAV Industry. Shenzhen: Huifei UAV Application Technology Training Center, 2019

[5] Lan Y B, Chen S D. Current status and trends of plant protection UAV and its spraying technology in China. Int J Precis Agric Aviat, 2018; 1(1): 1–9. doi: 10.33440/j.ijpaa.20180101.0002

[6] Li J, Lan Y, Shi Y. Research progress on airflow characteristics and field pesticide application system of rotary-wing UAV. Transactions of the Chinese Society of Agricultural Engineering, 2018; 34(12): 104–118.

[7] Li J, Yao W, Lin J, et al. Three-dimensional wind field measurement system suitable for unmanned aerial vehicles and its use method: CN201610973681.9. 2017-05-17

[8] Li J, Lin J, Lan Y, et al. Wind field measurement platform under drone rotor wing and wind field measurement method using the platform: CN201710151904.5. 2017-08-18

[9] Li J, Huang C, Lan Y, et al. A zero-point adjustable dynamic pressure type wind speed measuring device: CN201610983366.4. 2017-04-19.

[10] Hu L, Zhou Z, Luo X, et al. Design and test of wireless sensor network measurement system for unmanned helicopter wind farm. Transactions of The Chinese Society of Agricultural Machinery，2014; 45(5): 221–226.

[11] Wang P, Hu L, Zhou Z, et al. Wind field measurement for supplementary pollination in hybrid rice breeding using unmanned gasoline engine single-rotor helicopter. Transactions of the Chinese Society of Agricultural Engineering, 2013; 29(3): 54–61.

[12] Li J, Zhou Z, Lan Y, et al. Distribution of canopy wind field produced by rotor unmanned aerial vehicle pollination operation. Transactions of the Chinese Society of Agricultural Engineering, 2015; 31(3): 77–86.

[13] Li J, Zhou Z, Hu L, et al. Optimization of operation parameters for supplementary pollination in hybrid rice breeding using round multi-axis multi-rotor electric unmanned helicopter. Transactions of the Chinese Society of Agricultural Engineering, 2014; 30(11): 1–9.

[14] Li J, Lan Y, Wang J, et al. The distribution of rice pollen based on a small UAV wind field. China Agricultural Abstracts-Agricultural Engineering, 2018; 30(02): 13–19. Available online:

[15] Liu X. Research on distribution regularity of downwash airflow velocity in rotor flow field of single rotor plant protection UAV. Heilongjiang Bayi Agricultural University, 2019;

[16] Tang, Q, et al. Numerical simulation of the downwash flow field and droplet movement from an unmanned helicopter for crop spraying. Computers and Electronics in Agriculture, 2020; 174:105468.

[17] Tang, Q, et al. High-accuracy, high-resolution downwash flow field measurements of an unmanned helicopter for precision agriculture. Computers and Electronics in Agriculture, 2020; 173:105390. doi: 10.1016/j.compag.2020.105468

[18] Tang, Q, et al. Application of an ultrasonic anemometer array to field measurements of the downwash flow of an agricultural unmanned helicopter. Transactions of the ASABE, 2019; 62 (5): 1219–1230.

[19] Wen S, Han J, Lan Y, et al. Influence of wing tip vortex on drift of single rotor plant protection unmanned aerial vehicle. Transactions of the Chinese Society for Agricultural Machinery, 2018; 49(8): 127–137.

[20] Yang F, Xue X, Cai C, et al. Effects of down wash airflow in hover on droplet motion law for multi-rotor unmanned plant protection machine. Transactions of the Chinese Society of Agricultural Engineering, 2018; 34(2): 64–73.

[21] Zhang H, Qi L, Wu Y, et al. Distribution characteristics of rotor downwash airflow field under spraying on orchard using unmanned aerial vehicle. Transactions of the Chinese Society of Agricultural Engineering, 2019; 35(18): 44–54.

[22] Wen S, Han J, Ning Z, et al. Numerical analysis and validation of spray distributions disturbed by quad-rotor drone wake at different flight speeds. Computers and Electronics in Agriculture, 2019; 166: 105036. doi: 10.1016/j.compag.2020.105468